Chemical Science

Accepted Manuscript

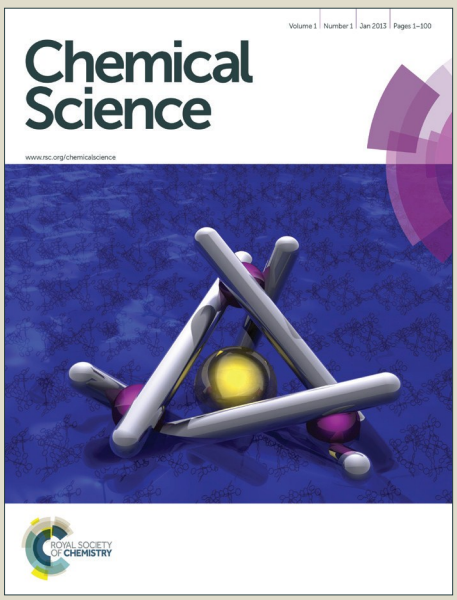

ROYAL SOCIETY OF CHEMISTRY

www.rsc.org/chemicalscience

Journal Name

RSCPublishing

EDGE ARTICLE

Fabrication of an Anti-Tumor Drug into Nanocrystalline Assemblies for Sustained Drug Release†

Cite this: DOI: 10.1039/xoxxoooooox

Received ooth January 2012,
Accepted ooth January 2012

DOI: 10.1039/xoxxoooooox

www.rsc.org/

Xiangrui Yang,[a‡] Shichao Wu,[a, b‡] Yang Li,[a, b] Huang Yu,[a] Di Chang,[a] Shefang Ye,[a] Liya Xie,[c] Yuan Jiang,*[a] and Zhenqing Hou*[a]

The delicate mesoscopic architectures, bearing complex forms with multiple hierarchy levels, lead to significant functions in biogenic minerals. Herein, a bio-inspired approach was developed to fabricate the comet-shaped assemblies of an anti-tumor drug – 10-hydroxycamptothecin (HCPT). The anti-solvent co-precipitation of HCPT and the excipient – PEG-*b*-PLGA within the emulsifier leads to the immediate nucleation of comet bundles, followed by the secondary nucleation to generate a comet head, which are assemblies of nanofibers aligned almost in parallel. The continuous manufacturing obtains drug-excipient hybrid particles with high drug-loading and sustained drug release profile. This simple and efficient bio-inspired approach led to a promising sustained local drug delivery system, and could be extended to fabrication of other functional organic materials bearing mesoscopic structural units.

Introduction

The delicate hierarchical architectures of biogenic materials across meso- and macro-scales suggest the existence of an alternative non-classical crystallization route[1]. Instead of passing through the straightforward classical crystallization pathway, where crystals grow via atomic/molecular attachments, the precursor formation and transformation into crystalline species are pivotal in non-classical crystallization routes. Non-classical crystallization, usually a multistage process, not only dominates in biomineralization[1, 2], but was overlooked in normal crystallization procedures for a long time. The precursors could have multiple forms. They could be non-crystalline species including clusters[3-6], amorphous nanoparticles[7-9], or liquid-like droplets[10-13]. In addition, they can be crystalline in form including nanocrystals[14-17] or mesocrystals[18, 19]. The transient existing precursors pass through the coupled crystallization-assembly process before reaching the thermodynamically stable crystalline form[19, 20]. For instance, the precipitation of alanine within the proper pH range could pass through the porous mesocrystalline state, as detected by the small-angle neutron scattering technique[19]. Soft ingredients can be actively involved via the chemical modification with supramolecular side chains or the physical adsorption of surfactants or polyelectrolytes. Both possibilities enrich the multistage crystallization pathways and the structural outcomes via stabilizing nanospecies and guiding the assembly behavior of the target compounds[21-24]. For instance, supramolecular porphyrins can assemble into nanofibers, which continue assembling spatially into microplatelets under the guidance of a block copolymer additive – Pluronic F127[22]. As comparison, supramolecular porphyrin would grow into bulk crystals without the amphiphilic additive[24]. The fabrication of functional materials via multistage crystallization pathways is promising to achieve advanced materials bearing rich mesoscopic forms and functions closely related to their mesoscopic structural forms.

For instance, multistage crystallization could have a profound and lasting impact on nanodrug manufacturing[25]. Nevertheless, there exist two main hurdles in fabrication of nanodrugs: the involvement of a high amount of surfactants as stabilizers and the long-term instability of nanodrugs. Hence, the manipulation of nanodrugs with high drug loadings and high stability is of great importance. Fabrication of nanospecies into assemblies would be a promising option, where a small amount of stabilizers including surfactants[22, 26], polyelectrolytes[27-30], and (block) copolymers[22, 31] could provide the colloidal forces to stabilize the assemblies and to prevent adjacent nanocrystals from merging into continuous architectures. This approach has been successful in fabrication of a series of functional materials including metal oxide[32], organics[29, 31], metal carbonates/phosphates[23, 33] into assemblies of nanocrystals. Significantly, the assembly could be well guided by external fields, which could induce the translational and orientational order into the assembly at the initial assembly stage[34, 35]. Unlike their nanocrystalline

[a]*Institute of Soft Matter and Biomimetics, College of Materials, Xiamen University, Xiamen 361005, China. E-mail: houzhenqing@xmu.edu.cn, yuan.jiang@xmu.edu.cn. Fax: +(86)592-2183058*
[b]*Department of Chemistry, College of Chemistry & Chemical Engineering, Xiamen University, Xiamen 361005, China*
[c]*The First Affiliated Hospital of Xiamen University, Xiamen University, Xiamen 361005, China*
†Electronic supplementary information (ESI) available. See DOI: 10.1039//b000000x
‡These authors contributed equally to this work

counterparts, assemblies of nanocrystalline drugs, usually micrometers in size, are advantageous for separation with the current tools and could be a clever option to escape from the nanotoxicity problems.

Here, we report the fabrication of assemblies of nanocrystalline 10-hydroxycamptothecin (HCPT) – a promising broad-spectrum anti-tumor agent with remarkable success in early clinical trials – via a multistage crystallization process. The anti-solvent co-precipitation of the HCPT and the excipient – PEG-*b*-PLGA[36-38] (monomethoxy polyethylene glycol–block–poly (lactide-co-glycolide) (PEG: 10 wt%, 5000 Da; PLGA: 90 wt%, 28000 Da) leads to nucleation of hybrid nanofibers with nanocrystalline HCPT as the core wrapped with different amounts of PEG-*b*-PLGA as steric stabilizers, depending on the initial ratios of API/excipient. Simultaneously, the flow within the channels of the emulsifier induces the spatial alignment of nanofibers into assemblies several micrometers in size. Delightfully, the continuous manufacturing of assemblies of nanocrystalline HCPT in a one-step process achieves HCPT–PEG-*b*-PLGA hybrid assemblies with the enhanced effect of sustained drug release for tumor treatments compared to their both nanocrystalline and bulk counterparts.

Results and discussion

A key feature of these experiments is performing the anti-solvent crystallization within a SPG membrane emulsification kit (SPG Technology Co. Ltd., Miyazaki, Japan). Both HCPT and PEG-*b*-PLGA were first dissolved in acetone and stored as the dispersion phase. Afterwards, a high pressure N_2 flow pushed the dispersion solution through the SPG membrane to enter the bulk aqueous phase, which is a poor solvent for both HCPT and PEG-*b*-PLGA. Due to the good miscibility between water and acetone and the existence of the strong fluid force, the concentration gradient of the solvent mixture was readily achieved in the exit area of each channel. Hence, the nucleation of HCPT nanofibers and the accompanying coprecipitation of PEG-*b*-PLGA onto the growing HCPT nanofibers presumably occurred in the exit area where the steep increase of the water content immediately increased the local supersaturation of both components to generate the coprecipitation. The dynamic nucleation and precipitation of nanospecies within the channel, plus the active occlusion of the soft ingredient – PEG-*b*-PLGA and the experimental conditions used, led to assemblies of nanocrystalline HCPT with tunable morphological character and componential distribution.

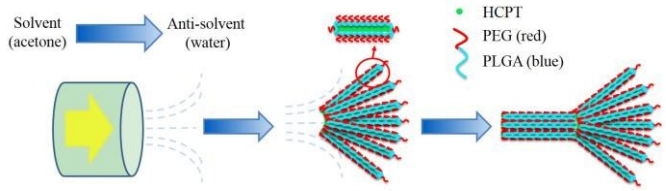

Scheme 1. Illustration of the multistage crystallization of the comet-shaped particles within the emulsifier. The color gradient in the blue arrow indicates the increase of the HCPT supersaturation, which increases with brighter color.

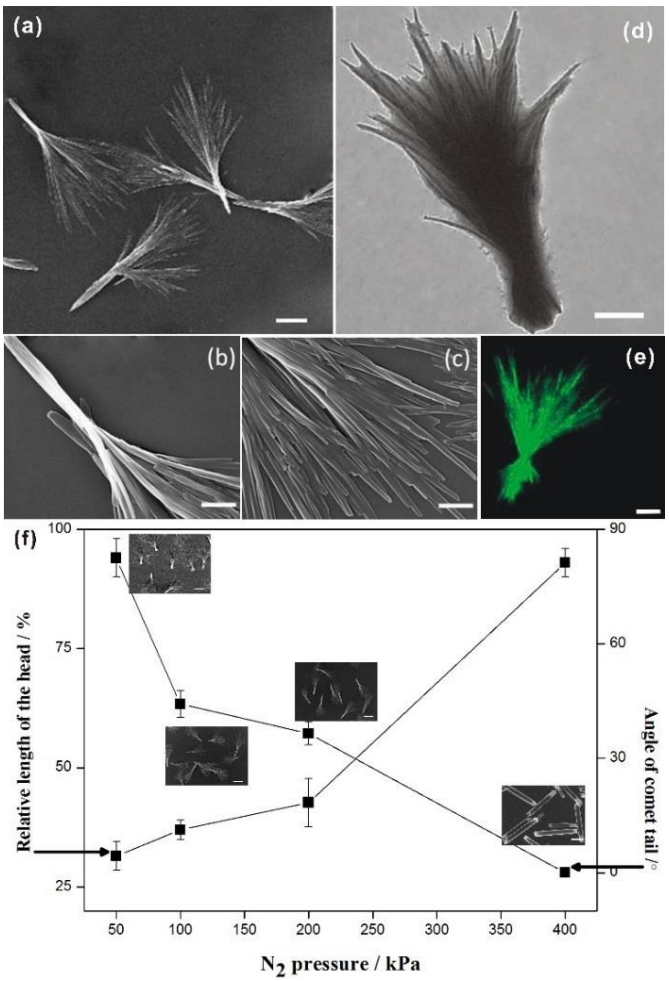

Figure 1. Images **a**-**e** illustrate the morphology of comet-shaped particles. The SEM image **a** is an overview of comet-shaped particles. The SEM images **b** and **c** show the structural details of a particle. Images **d** and **e** are TEM and CLSM images of a comet-shaped particle. The scale bars in **a**-**e** are 5 μm, 700 nm, 500 nm, 2 μm, and 2 μm. Image **f** is a diagram with the corresponding SEM images, indicating the relationship between the N_2 pressure and the tail angle (the left axis) and the relative length (head/tail) of the comet head (the right axis). The scale bars of SEM images in **f** are 5 μm.

A multistage crystallization pathway was proposed to form the comet-shaped particles (Scheme 1). Although the coprecipitation of PEG-*b*-PLGA molecules due to its insolubility in water coats a thin layer of block copolymers onto the growing HCPT nanofibers, its unsymmetric distribution on nanofibers still allow for the further growth of hybrid nanofibers on both ends, where the polymer density is relatively low. Considering that the crystallization depletes the HCPT molecules surrounded, the further growth of nanofibers prefers to occur in the rear area (the head of each bundle) to form the comet head, composed of almost parallel-aligned nanofibers, due to the high local supersaturation. The morphological details may vary according to the experimental conditions, which will be discussed together with microscopic images. The assemblies are permanently preserved because of the strong depletion force between adjacent nanofibers in analogy to porphyrin microplatelets[22] and $BaSO_4$ fiber bundles[39]. The existence of the external fluid force is crucial for the morphological control in the multistage crystallization

process. As comparison, the anti-solvent coprecipitation of HCPT and PEG-*b*-PLGA in the bulk phase under the stagnant condition led to spherulitic microspheres (see in the SI material). The insertion of the sonication produced a dispersion containing well-dispersed hybrid nanorods, which slowly aggregated after the sonication force was removed (see in the SI material). Hence, the dynamic solvent mixing at the interface between the membrane and the aquous phase is responsible for the comet-like shape.

Nevertheless, there could be another scenario of the multistage crystallization, which indicates the formation of the comet head within the channel followed by the crystallization of the comet tail. A simple experiment was designed to exclude this possibility. Instead of using the HCPT–PEG-*b*-PLGA acetone mother liquor as the dispersion phase, we pumped the freshly prepared HCPT nanorod acetone-water dispersion through the filter membrane with the similar diameter and checked the morphology of the collected particles. All particles obtained are dumbbell-shaped particles with a spherulitic tail on each end, suggesting that the crystallization occurs on both ends of nanorods in the exit area of the channel followed by the overgrowth of nanofibers in the tails (see in the SI material). This result unambiguously excludes the second pathway because the nucleation within the channel will still achieve comet-shaped particles with the prolonged comet head after passing through the channel.

The existence of PEG-*b*-PLGA possibly may not change either the crystal form or morphology of HCPT because a similar procedure without PEG-*b*-PLGA also passes through nanofibers before recrystallizing into bulk crystals. In each hybrid nanofiber, the PLGA chains prefer attaching to the inner HCPT nanofibers due to their hydrophobicity, while the short PEG segment (5000 Da) is exposed to water owing to its relative hydrophilicity and serves as the temporary steric stabilizer to stabilize the hybrid nanofibers from too fast and uncontrolled aggregation. This temporary stabilization was already utilized for inorganic nanocrystals by double hydrophilic block copolymers to allow controlled superstructure formation[40]. For these polymers, PEG blocks with a length of 3000 – 5000 g/mol were applied and striking examples of nanocrystal superstructures exist including $BaSO_4$ fiber bundles[39].

The structural details of comet-shaped particles were well recorded by optical and electron microscopes. SEM images show that particles are 10-15 μm in length with the width of the comet head about 400 nm in size. Particularly, the comets' tail consists of a bundle of nanofibers aligning radiated from the main body of the particle. Interestingly, the shape of the tail is determined on the flow rate controlled by the N_2 pressure. Increasing the N_2 pressure causes a decreased angle of the tail and an increased length of the comet head, as shown in Figure 1f. The angle of the tails and the length of the head reflect the flow rate-determined crystallization of the growing HCPT nanofibers into the bulk aqueous phase. Hence, nanofibers in the tail certainly spend limited time in the supersaturated regime to grow fully, and comet-like particles with a narrow tail is obtainable. Additionally, the strong flow rate during the crystallization also assists to obtain the relatively narrow tails. The limited time in crystallization under the strong N_2 pressure leaves the HCPT supersaturation in the acetone-water mixture relatively high. Thus, the long comet head is achieved. In an extreme case, the tail area almost disappears when the N_2 pressure is as high as 400 kPa (see in the SI material). Interestingly, the nanofibers in the comet head are partially merged into single crystalline architectures because of plenty time for the growth of the comet head and the limited protection from PEG-*b*-PLGA, in analogy to supramolecular porphyrin growing lacking enough amphiphilic additives[24]. The single crystalline microfibers, owing to their limited surface area, showed the decreased drug release effect compared with their comet-shaped counterparts (see single crystalline properties of microfibers in the polarized optical microscopic images in the SI material). So such particles are not assemblies of nanocrystals and hence, have been excluded from drug delivery experiments.

The coprecipitation of HCPT and PEG-*b*-PLGA produces hybrid particles with a variable drug loading from 11.9 % to 48.3 %. To obtain the highest entrapment efficiency and drug-loading content, an orthogonal L9 (3^3) test was designed to optimize the formulation conditions (see in the SI materials). The highest values of the entrapment efficiency and the drug loading value are 96.6 % and 48.3 %, respectively, under the experimental conditions as follows: HCPT / PEG-*b*-PLGA = 1 / 1 in mole; N_2 pressure = 100 kPa; SPG membrane with the pore size = 1.1 μm. The drug-loading efficiency was significantly enhanced compared with the value at about 5% by using the traditional methods[38, 41].

As is well-known, the form of drugs is an important factor that affects the drug release profile. Thus, it is of high importance to know the form of HCPT, i.e. a solid solution with PEG-*b*-PLGA, amorphous phase, or crystalline form. Although the comet-shaped particles show birefringent properties under the polarized optical microscope, the particles are too small to achieve good quality images. The X-ray diffraction was used to detect the form of HCPT within the hybrid particles (see in the SI materials). In addition to one representative peak attributed to the semicrystalline PEG-*b*-PLGA, a majority of peaks in the XRD pattern of the hybrid particles belong to HCPT, suggesting its high crystallinity. Moreover, the HCPT within the hybrid particles shows the same polymorph as their bulk counterparts. In short, the XRD results nicely suggest that the multistage crystallization mainly changes the growth kinetics of HCPT with the active occlusion of PEG-*b*-PLGA and the confining effects of the emulsifier.

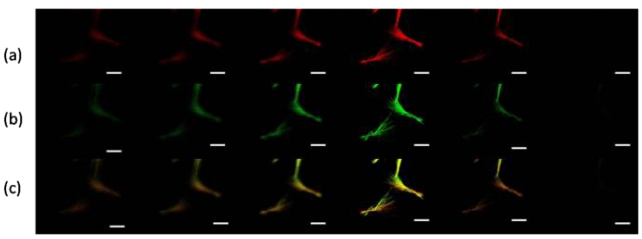

Figure 2. Z-scanning Confocal laser scanning microscopic images of comet-shaped particles. The images from left to right are imaged from top to bottom of the particle. **a**) Red fluorescence of Rhodamine B labeled PEG-*b*-PLGA; **b**) Green fluorescence of HCPT; **c**) The merged image of **a** and **b**. Scale bar is 5 μm.

Next, the distribution of HCPT and PEG-*b*-PLGA within the hybrid particles has been analyzed by using the Z-scanning imaging systems in the Confocal laser scanning microscopy (CLSM, Olympus FV1000; Figure 2). The green fluorescence imaging (excitation at 382 nm) was performed to visualize HCPT in the comet-shaped particles. The result nicely indicates that HCPT is uniformly distributed within the particle. To facilitate

the observation of PEG-*b*-PLGA under the CLSM, the polymer was labelled with Rhodamine B by the carbonyldiimidazole-mediated method (see in the SI materials). Excitingly, the red fluorescence (excitation at 555 nm) overlaps nicely with the green one, presenting the homogeneous distribution of both ingredients. The TEM image clearly indicates that nanofibers are wrapped by a thin layer of soft ingredients, presumably PEG-*b*-PLGA (Figure 1d). The two characterization results lead to the core-shell architectures of the nanofibers: the crystalline HCPT forms the core, while the shell is mainly composed of PEG-*b*-PLGA to enhance the steric stabilization of the hybrid particles in the dispersion.

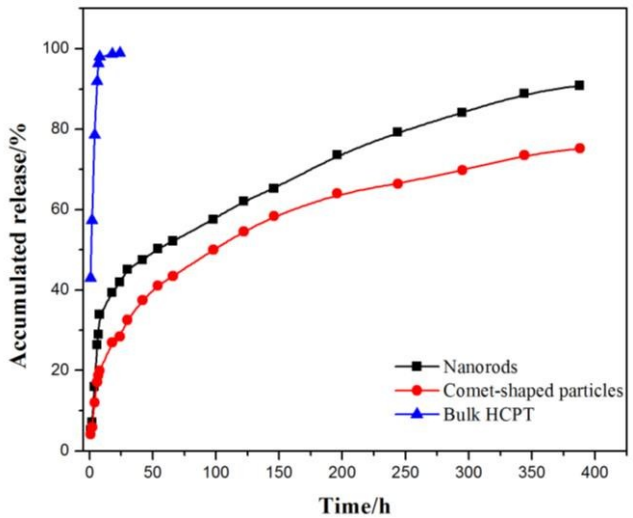

Figure 3. *In-vitro* release profiles of comet-shaped particles, nanorods, and commercial bulk HCPT powders.

The core-shell architectures of hybrid particles allow the sustained release of HCPT. The *in vitro* release studies of the comet-shaped particles (drug loading at 16.2 wt%) were performed using a dialysis technique, alongside with the nanorods collected from the sonication-assisted precipitation (15.0% content) and bulk HCPT powders. All samples were assayed by fluorescence spectrophotometry (excitation at 382 nm). The release profiles of HCPT are shown in Figure 3. The bulk HCPT was almost completely released within 24 h. As comparison, both hybrid particles and nanorods exhibit a remarkably prolonged release profile over a period of 400 h because of the diffusion limitation provided by the polymeric shell. In addition, unlike nanorods, which have a significant burst release in the initial stage, hybrid particles exhibit a steady sustained release pattern throughout the releasing period. We expect that the spatial alignment of nanofibers in the assembly effectively reduces the initial burst release compared with isolated nanorods with the similar drug loading value, though a well-established study showed that drug release could also be controlled by the drug loading content of particles[42].

The manufacturing of the core-shell hybrid particles provides a growing number of opportunities for HCPT from the practical point of view. Importantly, the anti-tumor effect of HCPT is both dose- and time-dependent[43]. Due to its practical insolubility in the aqueous phase, people use its soluble carboxylate form for clinical treatments, usually for intravenous administration. Nevertheless, the carboxylate form of HCPT shows a decreased activity compared to the underivatized molecule. Other approaches have the difficulty to achieve high drug loading formulations[38, 41]. Promisingly, the sustained drug releasing properties and the good colloidal stability of our core-shell hybrid particles allow for the local injection of the particle dispersion directly around the tumor area for the sustained release at relatively low concentration. Our cytotoxicity experiments nicely indicate that the hybrid particles show the enhanced cytotoxicity (BEL-7402) compared with the commercial HCPT (the hydroxycamptothecin injection) and the colloidal PEG-*b*-PLGA (see in the SI materials).

Conclusions

The study herein presents a simple and effective approach to obtain the comet-shaped drug-excipient hybrid particles with the high drug-loading content and sustained release properties. The comet-shaped HCPT–PEG-*b*-PLGA particles are promising as sustained local drug delivery system for the treatment of tumor. The animal experiments are going on now. Fabrication of nanodrugs into assemblies via bio-inspired crystallization approaches opens door to grow mesoscopic architectures of nanodrugs, which are convenient for separation with the current separation tools and for reducing the side effects compared to dispersions containing kinetically stable isolated nanodrug particles. Coprecipitation of drug with excipient provides an efficient continuous manufacturing strategy to produce a new generation of drugs with high stability.

Acknowledgements

This work is supported by the National Natural Science Foundation of China (21303144), Science Foundation of the Fujian Province, China (2014J0101), and Scientific Research Staring Foundation for the Returned Overseas Chinese Scholars, Ministry of Education of China. We thank Prof. Dr. Helmut Cölfen for the mechanistic discussions and constructive suggestions.

Notes and references

1. F. C. Meldrum and H. Cölfen, *Chem. Rev.*, 2008, **108**, 4332-4432.
2. Y. Oaki and H. Imai, *Adv. Funct. Mater.*, 2005, **15**, 1407-1414.
3. D. Gebauer, A. Völkel and H. Cölfen, *Science*, 2008, **322**, 1819-1822.
4. D. Erdemir, A. Y. Lee and A. S. Myerson, *Acc. Chem. Res.*, 2009, **42**, 621-629.
5. E. M. Pouget, P. H. H. Bomans, J. Goos, P. M. Frederik, G. de With and N. Sommerdijk, *Science*, 2009, **323**, 1455-1458.
6. D. Gebauer, M. Kellermeier, J. D. Gale, L. Bergström and H. Cölfen, *Chem. Soc. Rev.*, 2014, **43**, 2348-2371.
7. L. Addadi, S. Raz and S. Weiner, *Adv. Mater.*, 2003, **15**, 959-970.
8. Y. Politi, T. Arad, E. Klein, S. Weiner and L. Addadi, *Science*, 2004, **306**, 1161-1164.
9. S. E. Wolf, J. Leiterer, M. Kappl, F. Emmerling and W. Tremel, *J. Am. Chem. Soc.*, 2008, **130**, 12342-12347.
10. O. Galkin and P. G. Vekilov, *Proc. Natl. Acad. Sci. U.S.A.*, 2000, **97**, 6277-6281.
11. L. B. Gower and D. J. Odom, *J. Cryst. Growth*, 2000, **210**, 719-734.
12. P. G. Vekilov, *Cryst. Growth Des.*, 2004, **4**, 671-685.
13. M. A. Bewernitz, D. Gebauer, J. Long, H. Cölfen and L. B. Gower, *Faraday Discuss.*, 2012, **159**, 291-312.
14. J. F. Banfield, S. A. Welch, H. Z. Zhang, T. T. Ebert and R. L. Penn, *Science*, 2000, **289**, 751-754.
15. M. Niederberger and H. Cölfen, *Phys. Chem. Chem. Phys.*, 2006, **8**, 3271-3287.
16. H. Zheng, R. K. Smith, Y.-w. Jun, C. Kisielowski, U. Dahmen and A. P. Alivisatos, *Science*, 2009, **324**, 1309-1312.

17. D. Li, M. H. Nielsen, J. R. I. Lee, C. Frandsen, J. F. Banfield and J. J. De Yoreo, *Science*, 2012, **336**, 1014-1018.
18. Y. R. Ma, H. Cölfen and M. Antonietti, *J. Phys. Chem. B*, 2006, **110**, 10822-10828.
19. D. Schwahn, Y. Ma and H. Cölfen, *J. Phys. Chem. C*, 2007, **111**, 3224-3227.
20. V. M. Yuwono, N. D. Burrows, J. A. Soltis and R. L. Penn, *J. Am. Chem. Soc.*, 2010, **132**, 2163-2165.
21. V. Pipich, M. Balz, S. E. Wolf, W. Tremel and D. Schwahn, *J. Am. Chem. Soc.*, 2008, **130**, 6879-6892.
22. S. J. Lee, J. T. Hupp and S. T. Nguyen, *J. Am. Chem. Soc.*, 2008, **130**, 9632-9633.
23. S.-S. Wang, A. Picker, H. Cölfen and A.-W. Xu, *Angew. Chem. Int. Ed.*, 2013, **52**, 6317-6321.
24. X. Zhang, D. Gorl, V. Stepanenko and F. Wurthner, *Angew. Chem. Int. Ed.*, 2014, **53**, 1294-1298.
25. J. Chen, B. Sarma, J. M. B. Evans and A. S. Myerson, *Cryst. Growth Des.*, 2011, **11**, 887-895.
26. M. Li, H. Schnablegger and S. Mann, *Nature*, 1999, **402**, 393-395.
27. S. Wohlrab, H. Cölfen and M. Antonietti, *Angew. Chem. Int. Ed.*, 2005, **44**, 4087-4092.
28. Y. Jiang, H. F. Gong, D. Volkmer, L. Gower and H. Cölfen, *Adv. Mater.*, 2011, **23**, 3548-3552.
29. Y. Jiang, L. Gower, D. Volkmer and H. Cölfen, *Cryst. Growth Des.*, 2011, **11**, 3243-3249.
30. Y. Jiang, H. F. Gong, M. Grzywa, D. Volkmer, L. Gower and H. Cölfen, *Adv. Funct. Mater.*, 2013, **23**, 1547-1555.
31. Y. Ma, G. Mehltretter, C. Plueg, N. Rademacher, M. U. Schmidt and H. Cölfen, *Adv. Funct. Mater.*, 2009, **19**, 2095-2101.
32. Z. Bian, T. Tachikawa, P. Zhang, M. Fujitsuka and T. Majima, *Nature Commun.*, 2014, **5**, 3038.
33. T. X. Wang, H. Cölfen and M. Antonietti, *J. Am. Chem. Soc.*, 2005, **127**, 3246-3247.
34. A. Ahniyaz, Y. Sakamoto and L. Bergström, *Proc. Natl. Acad. Sci. U.S.A.*, 2007, **104**, 17570-17574.
35. R. van Hameren, P. Schon, A. M. van Buul, J. Hoogboom, S. V. Lazarenko, J. W. Gerritsen, H. Engelkamp, P. C. M. Christianen, H. A. Heus, J. C. Maan, T. Rasing, S. Speller, A. E. Rowan, J. Elemans and R. J. M. Nolte, *Science*, 2006, **314**, 1433-1436.
36. F. Danhier, E. Ansorena, J. M. Silva, R. Coco, A. Le Breton and V. Préat, *J. Controlled Release*, 2012, **161**, 505-522.
37. S. Dhar, F. X. Gu, R. Langer, O. C. Farokhzad and S. J. Lippard, *Proc. Natl. Acad. Sci. U.S.A.*, 2008, **105**, 17356-17361.
38. T. Govender, S. Stolnik, M. C. Garnett, L. Illum and S. S. Davis, *J. Controlled Release*, 1999, **57**, 171-185.
39. L. M. Qi, H. Cölfen and M. Antonietti, *Angew. Chem. Int. Ed.*, 2000, **39**, 604-607.
40. H. Cölfen, *Macromol. Rapid Commun.*, 2001, **22**, 219-252.
41. M. H. Hong, S. J. Zhu, Y. Y. Jiang, G. T. Tang and Y. Y. Pei, *J. Controlled Release*, 2009, **133**, 96-102.
42. J. M. Pang, Y. X. Luan, F. F. Li, X. Q. Cai, J. M. Du and Z. H. Li, *Int. J. Nanomed.*, 2011, **6**, 659-665.
43. D. Xiao, W. Tan, M. Li and J. Ding, *Life Sci.*, 2001, **69**, 1619-1628.